INTERNATIONAL JOURNAL OF AGRICULTURE & BIOLOGY
ISSN Print: 1560–8530; ISSN Online: 1814–9596
16–0034/2016/18–4–747–756
DOI: 10.17957/IJAB/15.0162
http://www.fspublishers.org

Full Length Article

Detection of Wheat Powdery Mildew by Differentiating Background Factors using Hyperspectral Imaging

Dongyan Zhang[1,2,3], Fenfang Lin[4], Yanbo Huang[5], Xiu Wang[2,3] and Lifu Zhang[1*]
[1]*State Key Laboratory of Remote Sensing Science, Institute of Remote Sensing & Digital Earth, Chinese Academy of Sciences, Beijing 100101, China*
[2]*Anhui Engineering Laboratory of Agro-Ecological Big Data, Anhui University, Hefei 230601, China*
[3]*Beijing Research Center for Information Technology in Agriculture, Beijing Academy of Agriculture and Forestry Sciences, Beijing 100097, China*
[4]*School of Geography and Remote Sensing, Nanjing University of Information Science & Technology, Nanjing 210044, China*
[5]*USDA-ARS Crop Production Systems Research Unit, Stoneville, MS 38776, USA*
[*]For correspondence: zhanglf@radi.ac.cn

Abstract

Accurate assessment of crop disease severities is the key for precision application of pesticides to prevent disease infestation. In-situ hyperspectral imaging technology can provide high-resolution imagery with spectra for rapid identification of crop disease and determining disease infestation trend. In this study a hyperspectral imager was used to detect wheat powdery mildew with considering the impacts of wheat ears and the leaves under shadow to identify infected and healthy plant leaves. Through comparing the spectral differences between wheat ears and shadowed, healthy and infected plant leaves, 23 sensitive bands were chosen to distinguish different background targets. Five vegetation indices (VIs) and three red edge parameters were calculated based on screened sensitive bands. Then, 40 identification features were determined to distinguish different background factors and disease severities. Moreover, the classification and regression tree (CRT) was utilized to develop the prediction model of wheat powdery mildew. The identification accuracy was assessed by cross-validation with the accuracies that shadowed leaves can be perfectly recognized while the healthy and infected leaves, wheat ears could be identified with the rates of 98.4, 98.4 and 80.8%, respectively. For identification of different disease severities, the healthy leaves have the highest accuracy with 99.2%, while moderately and mildly infected leaves were determined as 88.2 and 87.8%, respectively. In overall, it was found that wheat ears could affect identification accuracy of wheat powdery mildew. At the same time, in order to provide guidance for application of pesticides, improved accuracy for detecting mildly infected disease is expected. © 2016 Friends Science Publishers

Keywords: Wheat ear; Powdery mildew; Disease severities; Hyperspectral imaging

Introduction

Accurate assessment of crop diseases can provide decision support for the management of agricultural production. The assessment based on optical remote sensing could be valuable in reducing spray volume, improving crop quality, increasing yield, and serving for food security (Devadas *et al*., 2009). Wheat powdery mildew is caused by the *Erysiphe graminis*, which often infects the leaf blade and sheath. When the disease is severe, the stem and ear would also be infected. The disease reduces plant vigor and may result in being withered or even death by blocking leaf photosynthesis. This disease is especially harmful to wheat from the late heading growth stage to maturity (Giese *et al*., 1997). It is one of the most common wheat diseases in China. The disease has significantly negative effects on wheat yield and quality and surrounding environment (Huang *et al*., 2013).

The studies of spectral analysis on rice (Qin and Zhang, 2005; Yang, 2010), wheat (Ashourloo *et al*., 2014a; Zhao *et al*., 2014), cotton (Ortiz *et al*., 2011; Zhang *et al*., 2013) and corn crop (Chen *et al*., 2010) showed that pigments of plant leaves have sensitive response in the visible-light range of spectrum e.g., 400–750 nm, while the leaf and canopy structures have sensitive response in the near-infrared (NIR) spectrum of 750–1000 nm. The two spectrum ranges are the major sources of information for developing VIs (Vegetation Indices). The VIs developed in such a way have been widely used well in the scale of the crop leaf, canopy and field (Huang *et al*., 2007; Haboudane *et al*., 2008; Ashourloo *et al*., 2014b). Difference in spectral response of disease severities is the basis of optical diagnostics for crop diseases. Based on the spectral characteristics of disease, the sensitive bands of disease

To cite this paper: Zhang, D., F. Lin, Y. Huang and L. Zhang, 2016. Detection of wheat powdery mildew by differentiating background factors using hyperspectral imaging. *Int. J. Agric. Biol.*, 18: 747–756

identification are screened to build the indices to assess the diseases level. Devadas *et al.* (2009) calculated ten vegetation indexes to distinguish diseases of wheat (Devadas *et al*., 2009). The results showed that two vegetation indices, ARI (Anthocynanin Reflectance Index) and TCARI (Transformed Chlorophyll Absorption Ratio Index), could recognize wheat stripe rust accurately in the scale of leaf. Ashourloo *et al.* (2014c) used hyperspectral data to assess the different symptoms of wheat rust for wheat disease recognition using VIs (Ashourloo *et al*., 2014c; Huang *et al.*, 2015). They selected 455 nm, 605 nm and 695 nm as the disease sensitive bands and built a new VI of wheat rust detection. Huang *et al.* (2014) used the Relief-F algorithm to select the sensitive bands of wheat diseases. They proposed new VIs for wheat powdery mildew and wheat stripe rust. Their prediction model of wheat stripe rust was as high as 0.86.

The models for wheat disease have high accuracies in disease recognition in the scale of plant leaf. However, the generalization and robustness of the models have to be verified in the scale of field with the data across crop varieties (Devadas *et al*., 2009; Ashourloo *et al*., 2014a; Huang *et al*., 2014). Up to now, there are still few literatures focused on crop disease recognition and assessment in the scale of crop canopy and field (Ashourloo *et al*., 2014b). Devadas *et al.* (2009) found that healthy, diseased and shadowed leaves, wheat ear, wheat stems and soil constitutes a complex environmental background for wheat disease diagnosis in the field (Devadas *et al*., 2009). By investigating the influences of wheat ears, shadowed leaves, soil and other background factors, the model accuracy could be improved for wheat disease assessment in the scale of canopy and field (Huang *et al*., 2014). Due to the limitations in the development of sensors and instruments, there are few reports on the influences of the background factors to crop disease recognition. In this study, we used a hyperspectral imager to measure and analyze the impacts of the different factors on recognizing wheat powdery mildew. Specifically, we determined sensitive bands and related transformed features for detection of powdery mildew through correlation analysis and independent testing; furthermore, we built and verified decision tree models to differentiate background factors and determine wheat disease severities.

Materials and Methods

Experimental Setup

The experimental site is located at the experimental farm of Beijing Academy of Agriculture and Forestry Sciences (39° 56'N, 116°16'E). The wheat cultivar, Jingshuang16, which is highly sensitive to powdery mildew, was chosen as research target. The wheat was planted in October 2013. Regular fertilizer and irrigation treatments were conducted during the growth season. The wheat powdery mildew commonly outbreaks in the heading stage and the early grain filling stage in the area of Beijing, China, when the temperature ranges from 15 to 20°C with high relative humidity over 70%.

Data Acquisition and Processing

Equipment: The hyperspectral imager, SOC710VP (Surface Optics Corp., San Diego, CA, USA) was used to collect hyperspectral images of powdery mildew infected wheat plants. This instrument is a built-in scanning imaging system mounted with the C-Mount zoom lens, which is easy to adjust the amount of light exposure. When acquiring images each operation provides a pair of area-array images through the control of the software developed by the company, SOC. The technical parameters of the SOC710VP are shown in Table 1. In field operation the imager was placed at a portable and multifunction field observation bracket to capture canopy image after being adjusted to the optimal height and viewing angle through the built-in gradienter to ensure consistent field image collection.

Hyperspectral Image Acquisition

In this study, hyperspectral images of different disease severities were captured at the early and middle filling stage. The canopy images were collected from 10: 00 am to 13:30 pm under sunny and breeze conditions. The data collection process was as:

1). According to the severities of the disease, combined with the disease investigation criteria of the Ministry of Agriculture, China (Huang *et al*., 2014), the disease is divided into three levels, which includes a total of 30 sampling areas, 10 sampling points for each level.

2). According to the canopy height and the viewing angle of the instrument, the distance of 100 cm was set between lens to the surface of the canopy to cover the ground area of 50 by 50 cm.

3). Placed a reference board in the field of view to reduce the radiance correction error caused by sunlight before capturing each canopy image.

Data Processing

The hyperspectral image is processed in three steps: reflectance conversion, ROI (Region of Interest) extraction and image smoothing. In order to process data for model development, the data were further processed for selection of sensitive band, recognition feature extraction (VIs and calculation of red edge parameters). The data processing work flow is shown in Fig. 1.

Reflectance Conversion

The original DN (Digital Number) image was converted to a relative reflectance image through the third-party software ENVI (Exelis Visual Information Solutions, Boulder, CO,

USA) using the Flat Field (FF) method. In the study, the spectral values of relative reflectance were from 0 to 4. The FF (Flat Field) model was developed on the basis of the IARR (Internal Average Relative Reflectance) model. The IARR model was provided in the presence of a certain area of the image, and the mean distribution of the pure field units. Calculating the elements of pure feature in the mean spectrum, the spectrum of each image pixel values is divided by this mean spectrum, thereby achieving the relative reflectance. The expression of this model is:

$$R_j(i) = \left(\frac{N_j^a}{\sum_i DN_j(i^a)}\right) DN_j(i) \quad (1)$$

Where, $R_j(i)$ is the relative reflectance of j-th channel and the i-th pixel of the sensor; N^a_j is the number of pixel of pure feature units in j-channel sensor; $DN_j(i^a)$ indicates the DN value of i^a –th pixel in j-channel sensor of the pure feature units. $DN_j(i)$ is the DN value of the i-th pixel in the j-th channel of the sensor.

Extracting Regions of Interest

Due to one image consists of a variety of background targets; the relative reflectance of different targets can be extracted through the selection of ROIs. In this research, four kinds of ROIs were selected and saved, including infected-, healthy- and shadowed leaves (refer to block each blade caused by the shaded area), and wheat ears by using ENVI.

Smoothing Images

The moving average method was utilized to reduce the noise of hyperspectral image from the moisture and light in the field environment (Devadas *et al*., 2009). The smoothing step was set to 4.

Selection of Sensitive Bands

Due to each our hyperspectral image contains 128 bands, and between bands exist the strong correlation. Thus, processing all the band data all together would reduce the data processing efficiency and affect the recognition accuracy of wheat powdery mildew. Therefore, the data dimensionality should be reduced firstly. That means investigating the sensitivity of the 128 bands to identify the more sensitive and effective bands out of them. In this study, SPCA (Segmented Principal Component Analysis) was conducted to select the sensitive bands. Compared with the PCA (Principal Component Analysis), SPCA not only requires less amount of computation, but also avoids neglecting local characteristics. In addition, SPCA calculates the contribution of each band, not the main component of PCA, to reduce the dimensions. SPCA reserves the physical meaning of the reflectance of the field targets (Hemmateenejad *et al*., 2012).

According to the adjacent band correlation coefficients of hyperspectral images, the SPCA divides all bands into band groups, followed by PCA converting within each band group. After the converting of the principal components, the contribution for each band is calculated by using the sum square of the correlation coefficient for each band and the main components. Finally, the representative of each sub-band space is selected according to the contribution.

Band Operation

The single band is difficult to accurately identify and evaluate wheat diseases as the contained information is very limited. Studies have shown that once several sensitive bands are confirmed, the wheat powdery mildew could be diagnosed precisely by calculating a vegetation index (Mahlein *et al*., 2012). Table 2 shows several disease vegetation indexes (Devadas *et al*., 2009; Naidu *et al*., 2009; Ashourloo *et al*., 2014c). In order to enhance the disease features recognition; this study also used the red edge parameters, including the slope of the red edge, red edge position and the red edge area (Table 2) (Zhang *et al*., 2012).

Extracting Recognition Features

Sensitive bands were selected and we found that they were mostly located in the red and NIR band regions. Thus, there are many results of RVI (Ratio Vegetation Index) and NDVI (Normalized difference vegetation index), which contain the parameters is related or not obviously related to powdery mildew. In order to build the optimal assessment model, it is necessary to extract sensitive features of powdery mildew and background factors. The Stepwise Discriminant Analysis of Wilk's lambda statistic was used for selection of disease recognition features using the software SPSS (SPSS Inc., Chicago, IL, USA) (Field, 2013).

Model Development and Validation

In this study, we used CRT (Classification and Regression Tree) growth method to establish and verify the model by using the SPSS software. The CRT tree divides the data into several sections as homogeneous as possible with the dependent variables. All dependent variable values are in the same terminal node which is a homogeneous, "pure" node (Rokach and Maimon, 2008). The validation criteria were the split-sample select validation. That is, a randomly selected 70% samples were assigned as the training samples and the rest 30% were tested samples. Finally, the results of classification tree were output to evaluate recognition accuracy of the model.

Table 1: Technical parameters of SOC710VP hyperspectral imager

Spectral Coverage: 400–1000 nm	Pixels per line: 696
Spectral Resolution: 4.68 nm	Weight: 2.95 kg
Spectral Bands: 128	Focal Length: Configurable (based on lens used)
Dynamic Range: 12-bit	Power: 12-VDC / 100-240VAC (50-60Hz)
Lens Type: C-Mount	Dimensions (HWL): 9.5 x 16.8 x 22cm
Speed: 30 spatial lines per second	23.2 seconds/cube (696 by 520 cube)

Table 2: The VIs for detection of wheat powdery mildew

Index name	Formula	Relevant plant pigment	Reference
Ratio vegetation index	RVI	Reflectance ration of two bands, sensitive to disease stress	Qin *et al.* 2005
Normalized difference vegetation index	NDVI	NIR and Red are broad reflectance bands 775-825 nm, sensitive to disease stress	Devadas *et al.* 2009
Green normalized difference vegetation index	GNDVI	Defined as an index of plant "greenness" or photosynthetic activity, sensitive to disease stress	Ashourloo *et al.* 2014
Photochemical reflectance index	PRI	R531associated with state of the xanthophyll cycle and as xanthophyll pigments fulfill a photoprotective role, and key to light use efficiency (LUE)	Huang *et al.* 2007
Red-edge vegetation stress index	RVSI	$((R_{712} + R_{752})/2) - R_{732}$, sensitive to disease stress	Naidu *et al.* 2009
Red edge position	REP	REP represents certain wavelength position within the red edge (650—750 nm). Sensitive to disease stress	Devadas *et al.* 2009
Dr	Dr	Dr is a maximum value of 1st order derivatives within the red edge (650—750 nm). Sensitive to disease stress	Ashourloo *et al.* 2014
SDr	SDr	Defined by sum of 1st order derivative values within the red edge (650—750 nm), sensitive to disease stress	Ashourloo *et al.* 2014

Results

Spectral Response of Different Background Factors

Spectral response of diseased leaves: A wheat plant consists of the blade, stem, ear and other parts. There are different spectral response characteristics for different components in the specific growth stage, or in different stresses (Zhao *et al*., 2008). Hyperspectral data typically contain hundreds of spectral bands. The particular wavelength position can highlight detail spectral differences, which provides hints to distinguish disease stress and plant components (Mutka and Bart, 2014). Fig. 2b is the spectral response curves of diseased, healthy, shadowed leaves and wheat ear. The data were precisely extracted on the positions shown in Fig. 2a.

Fig. 2 shows significant spectral differences for the four measured targets in visible region of 400–700 nm, especially in the green and red bands (Zhang *et al*., 2012). Despite the shadowed leaf has the spectral response of vegetation, its magnitude is significantly lower than the other three, and the green peak of 550 nm is not prominent. Ear of wheat with reflection green peak and absorption red valley, also shows the obvious trend of red edge shifting to blue light direction. In the NIR region, there is a smooth high reflectance platform for healthy and shadowed leaves and wheat ear while the spectral values of diseased leaves go upward greatly. In addition, the reflectivity of healthy leaves and wheat ear is higher than diseased leaves. Near to water vapor absorption band of 960 nm, the spectral responses of four targets are different also. There are significantly deeper absorption valleys for diseased and shadowed leaves.

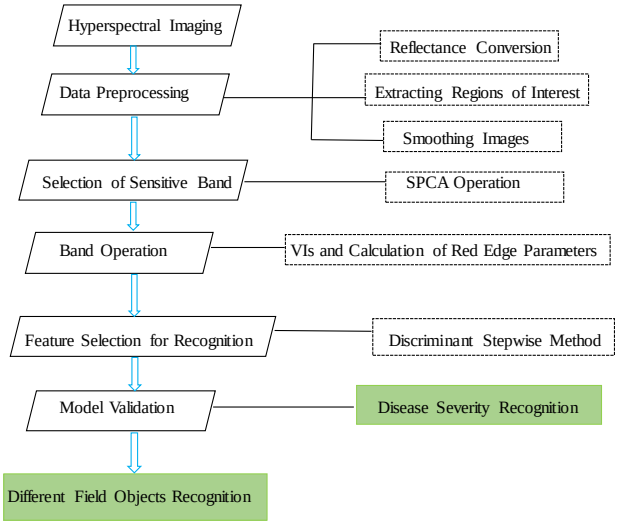

Fig. 1: Data processing work flow

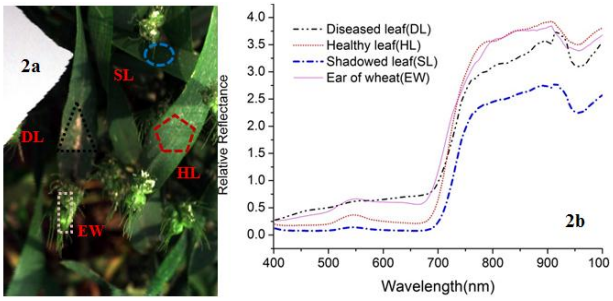

Fig. 2: Spectral response curves of diseased and healthy leaves and different background factors

Spectral response of disease severities: The absorption and reflection characteristics of vegetation would change in different spectral bands when the plants were infected with disease. Thus, the spectral responses of infected vegetation should be expressed as spectral features through certain data processing. This is the fundamental basis of optical remote sensing for assessment of disease severities of vegetation (Devadas *et al*., 2009; Zhang *et al*., 2012).

Fig. 3b shows the spectral response curves of different disease severities for the wheat powdery mildew (healthy, mild infected and moderate infected). The data was measured at the locations as shown in (Fig. 3a and b) shows that the curves have no obvious green peak (550 nm) and red valley (670 nm). However, they present differences in reflective intensity. These differences are useful for differentiation between infected and healthy leaves. Compared with healthy and mild infected leaves, the reflectance of moderate infected leaves goes upward rapidly in the NIR range. In addition, all the curves demonstrate differences in the reflectance intensity.

In overall, the spectral response difference not only presents between infected leaves and three background factors, but also in different disease severities, which provide a reference basis for further recognizing wheat powdery mildew based on sensitive band selection and feature parameter formulation.

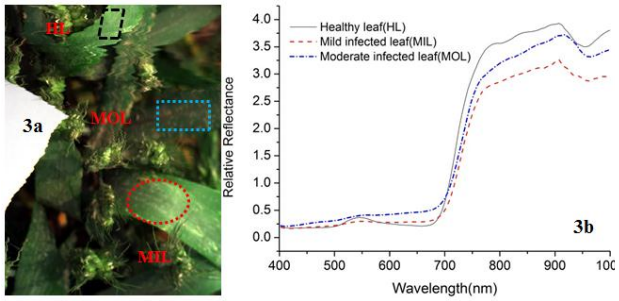

Fig. 3: Spectral curves of different disease severities

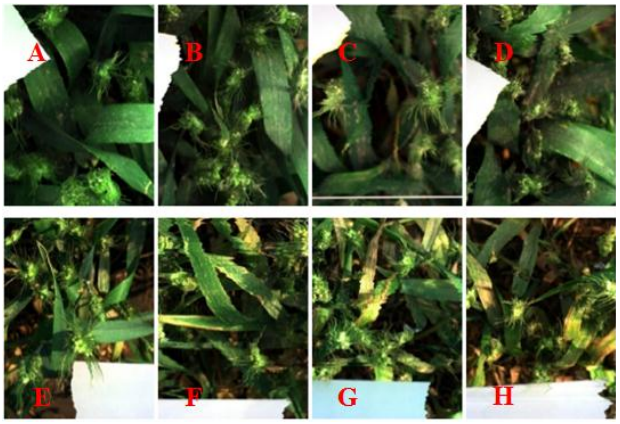

Fig. 4: Images of different sampling Points for different background factors and disease severities (White object is the spectral reference board)

Recognition Features of Disease

Sensitive band: Through calculating the contribution for all sample images from each subspace of each band using SPCA, we analyzed and compared variance significance to select sensitive bands between different background factors and disease severities. A total of 23 bands for the disease recognition are obtained (Table 3 and 4), which are 417 nm, 423 nm, 503 nm, 508 nm, 534 nm, 544 nm, 658 nm, 679 nm, 689 nm, 694 nm, 700 nm, 705 nm, 715 nm, 726 nm, 752 nm, 768 nm, 774 nm, 789 nm, 827 nm, 864 nm, 897 nm, 962 nm and 984 nm.

As seen in Table 3 and 4, there are 17 sensitive bands are mainly located in the red and NIR range, including 10 red edge bands. In addition, four bands are selected from green light region. Those are the ranges where the spectral responses are significantly different for different factors and disease severities. These bands are useful for computing disease recognition VIs and parameters, e.g. RVI, NDVI, GNDVI, PRI, RVSI, red edge position, red edge slope and red edge area (Table 2).

Recognition Features

Through screening over the results of VIs and red edge parameters using the stepwise discriminant method, 40 features were determined to be used for distinguishing four background factors and three disease severities (Table 5 and 6).

By analyzing disease recognition features in the Table 5 and 6, the features could be used to simultaneously distinguish the disease with different background factors and different severities, which are in the interval of 689~726 nm, the wavelength 768 nm and red edge area. The ratios of different combinations of feature bands are quite different. For example, 417 nm, 658 nm, and 789 nm were selected when distinguishing different background factors; and it does not appear in the recognizing different disease severities. However, the data in the Table 5 and 6 fully present a close relationship between red-edge spectral response and disease stress, which is consistent with other research results in the crop disease diagnosis (Devadas *et al*., 2009; Zhang *et al*., 2012).

Calibration and Validation of Disease Recognition Models

Based on the extracted recognition features, the discriminant models of different background factors and disease severities were respectively built using the CRT method. At the same time, the model accuracy to differentiate background factors was validated and shown in Table 7, while the accuracy to differentiate different disease severities is showed in Table 8.

Table 3: Variance analysis of sensitive wavebands between infected leaves and background targets

Factor band (nm)	Sensitive	Infected leaves			Healthy leaves			Shadowed leaves			Wheat ear		
		Healthy	Shadowed	Wheat ear	Infected	Shadowed	Wheat ear	Infected	Healthy	Wheat ear	Infected	Healthy	Shadowed
417	Ave	0.267*	0.148*	0.070*	-0.267*	-0.121*	-0.197*	-0.148*	-0.121*	-0.141*	-0.070	0.020*	0.141*
	p	0.000	0.000	0.066	0.000	0.000	0.000	0.000	0.000	0.000	0.066	0.000	0.000
423	Ave	0.383*	0.162*	0.013*	-0.038*	0.124*	-0.025*	-0.162*	-0.124*	-0.149*	-0.132*	-0.021*	0.149*
	p	0.000	0.000	0.001	0.000	0.000	0.000	0.000	0.000	0.000	0.001	0.000	0.000
503	Ave	0.139*	0.296*	-0.028*	-0.139*	-0.157*	-0.167*	-0.296*	-0.157*	-0.324*	0.028*	0.167*	0.324*
	p	0.000	0.000	0.000	0.000	0.000	0.000	0.000	0.000	0.000	0.000	0.000	0.000
508	Ave	0.137*	0.304*	-0.054*	-0.137*	0.167*	-0.192*	-0.304*	-0.167*	-0.359*	0.541*	0.192*	0.359*
	p	0.000	0.000	0.000	0.000	0.000	0.000	0.000	0.000	0.000	0.000	0.000	0.000
534	Ave	0.096*	0.330*	-0.197*	-0.096*	0.234*	-0.293*	-0.330*	-0.234*	-0.527*	0.197*	0.293*	0.527*
	p	0.000	0.000	0.000	0.000	0.000	0.000	0.000	0.000	0.000	0.000	0.000	0.000
544	Ave	0.098*	0.342*	-0.218*	-0.098*	0.244*	-0.315*	-0.342*	-0.244	-0.560*	0.218*	0.315*	0.560*
	p	0.000	0.000	0.000	0.000	0.000	0.000	0.000	0.000	0.000	0.000	0.000	0.000
658	Ave	0.337*	0.509*	0.100*	-0.337*	0.172*	-0.237*	-0.509*	-0.171*	-0.409*	-0.100*	0.237*	0.409*
	p	0.000	0.000	0.000	0.000	0.000	0.000	0.000	0.000	0.000	0.000	0.000	0.000
679	Ave	0.353*	0.542*	0.147*	-0.353*	0.189*	-0.205*	-0.542*	-0.189*	-0.394*	-0.149*	0.205*	0.394*
	p	0.000	0.000	0.000	0.000	0.000	0.000	0.000	0.000	0.000	0.000	0.000	0.000
689	Ave	0.346*	0.573*	0.039*	-0.346*	0.227*	-0.307*	-0.573*	-0.227*	-0.534*	-0.038*	0.307*	0.534*
	p	0.000	0.000	0.001	0.000	0.000	0.000	0.000	0.000	0.000	0.001	0.000	0.000
694	Ave	0.321*	0.602*	-0.051*	-0.321*	0.281*	-0.372*	-0.602*	-0.281*	-0.653*	0.051*	0.372*	0.653*
	p	0.000	0.000	0.000	0.000	0.000	0.000	0.000	0.000	0.000	0.000	0.000	0.000
700	Ave	0.266*	0.613*	-0.154*	-0.266*	0.346*	-0.420*	-0.613*	-0.346*	-0.766*	0.154*	0.420*	0.766*
	p	0.000	0.000	0.000	0.000	0.000	0.000	0.000	0.000	0.000	0.000	0.000	0.000
705	Ave	0.203*	0.623*	-0.260*	-0.203*	0.420*	-0.463*	-0.623*	-0.420*	-0.883*	0.260*	0.463*	0.883*
	p	0.000	0.000	0.000	0.000	0.000	0.000	0.000	0.000	0.000	0.000	0.000	0.000
715	Ave	0.053*	0.634*	-0.417*	-0.053*	0.581*	-0.471*	-0.634*	-0.581*	-1.051*	0.417*	0.471*	1.051*
	p	0.002	0.000	0.000	0.002	0.000	0.000	0.000	0.000	0.000	0.000	0.000	0.000
726	Ave	-0.18*	0.510*	-0.504*	0.178*	0.688*	-0.326*	-0.510*	-0.688*	-1.014*	0.504*	0.326*	1.014*
	p	0.000	0.000	0.000	0.000	0.000	0.000	0.000	0.000	0.000	0.000	0.000	0.000
752	Ave	-0.357*	0.419*	-0.441*	0.357*	0.776*	-0.085*	-0.419*	-0.776*	-0.860*	0.441*	0.085*	0.860*
	p	0.000	0.000	0.000	0.000	0.000	0.000	0.000	0.000	0.000	0.000	0.000	0.000
768	Ave	-0.392*	0.385*	-0.430*	0.392*	0.777*	-0.038*	-0.385*	-0.777*	-0.815*	0.430*	0.038*	0.815*
	p	0.000	0.000	0.000	0.000	0.000	0.115	0.000	0.000	0.000	0.000	0.115	0.000
774	Ave	-0.401*	0.382*	-0.437*	0.401*	0.782*	-0.036*	-0.382*	-0.782*	-0.819*	0.437*	0.036*	0.819*
	p	0.000	0.000	0.000	0.000	0.000	0.148	0.000	0.000	0.000	0.000	0.148	0.000
789	Ave	-0.417*	0.424*	-0.418*	0.417*	0.84*	-0.001*	-0.424*	-0.841*	-0.842*	0.418*	0.001*	0.842*
	p	0.000	0.000	0.000	0.000	0.000	0.977	0.000	0.000	0.000	0.000	0.977	0.000
827	Ave	-0.401*	0.479*	-0.376*	0.401*	0.880*	0.025*	-0.479*	-0.880*	-0.856*	0.376*	-0.025*	0.856*
	p	0.000	0.000	0.000	0.000	0.000	0.374	0.000	0.000	0.000	0.000	0.374	0.000
864	Ave	-0.381*	0.605*	-0.335*	0.381*	0.986*	0.046*	-0.605*	-0.986*	-0.940*	0.335*	-0.459*	0.940*
	p	0.000	0.000	0.000	0.000	0.000	0.094	0.000	0.000	0.000	0.000	0.094	0.000
897	Ave	-0.371*	0.735*	-0.267*	0.371*	1.106*	0.104*	-0.735*	-1.106*	-1.003*	0.267*	-0.104*	1.003*
	p	0.000	0.000	0.000	0.000	0.000	0.000	0.000	0.000	0.000	0.000	0.000	0.000
962	Ave	-0.289*	0.657*	-0.095*	0.289*	0.946*	0.194*	-0.657*	-0.946*	-0.752*	0.095*	-0.194*	0.752*
	p	0.000	0.000	0.000	0.000	0.000	0.000	0.000	0.000	0.000	0.000	0.000	0.000
984	Ave	-0.305*	0.764*	-0.133*	0.305*	1.069*	0.172*	-0.764*	-1.069*	-0.897*	0.133*	-0.172*	0.897*
	p	0.000	0.000	0.000	0.000	0.000	0.000	0.000	0.000	0.000	0.000	0.000	0.000

Note: The symbol * means the significance high than 0.05. (Ave – mean value; p – significant probability level)

As seen in Table 7 and 8, shadowed samples can be perfectly (100%) identified in the process of the distinguishing of background factors. The recognition accuracies for infected and healthy samples are the same as 98.4%. The accuracy of wheat ear is relatively low as 80.8%. In overall, the recognition model has a 95.6% accuracy and 95.2% kappa coefficient. In identification of powdery mildew severities, healthy samples had the highest recognition accuracy (99.2%); and the accuracies of the moderate and mild infected samples were 88.8 and 87.9%, respectively. Despite the discriminant accuracy of the model reaches 91.1% with 84.6% kappa coefficient, it is still lower than the accuracy to differentiate background factors, which might be mainly caused by the 68.3% accuracy in differentiating the mild infected samples.

The overall accuracy of two models is more than 90%, but the identification accuracy of wheat ear is obviously lower than the other three when differentiated background factors. The reason is that it has features of both healthy and more and more infected leaves, which interferes distinction of other factors. This can be clearly illustrated by the data in Table 7, where 91 samples of wheat ear are easily divided into the infected and healthy samples. For the recognition model of different disease severities, the accuracy of healthy samples is much higher than the other two infected levels, which means the diagnosis method is feasible for detecting the stress of wheat powdery mildew.

Table 4: Variance analysis of sensitive wavebands between different disease severities

Factor sensitive bands (nm)		Healthy		Mild		Moderate	
		Mild	Moderate	Healthy	Moderate	Healthy	Mild
417	Ave	-0.020*	-0.028*	0.020*	-0.008	-0.028*	0.008
	p	0.001	0.000	0.001	0.128	0.000	0.128
423	Ave	-0.024*	-0.042*	0.024*	-0.018*	0.042*	0.018*
	p	0.000	0.000	0.000	0.001	0.000	0.001
503	Ave	-0.105*	-0.148*	0.104*	-0.043*	0.148*	0.043*
	p	0.000	0.000	0.000	0.000	0.000	0.000
508	Ave	-0.106*	-0.146*	0.106*	-0.040*	0.146*	0.040*
	p	0.000	0.000	0.000	0.000	0.000	0.000
534	Ave	-0.084*	-0.099*	0.084*	-0.015	0.099*	0.015
	p	0.000	0.000	0.000	0.171	0.000	0.171
544	Ave	-0.087*	-0.101*	0.087*	-0.014	0.101*	0.014
	p	0.000	0.000	0.000	0.221	0.000	0.221
658	Ave	-0.220*	-0.369*	0.220*	-0.150*	0.369*	0.150*
	p	0.000	0.000	0.000	0.000	0.000	0.000
679	Ave	-0.222*	-0.389*	0.222*	-0.167*	0.389*	0.167*
	p	0.000	0.000	0.000	0.000	0.000	0.000
689	Ave	-0.225*	-0.379*	0.225*	-0.154*	0.379*	0.154*
	p	0.000	0.000	0.000	0.000	0.000	0.000
694	Ave	-0.204*	-0.353*	0.204*	-0.149*	0.353*	0.149*
	p	0.000	0.000	0.000	0.000	0.000	0.000
700	Ave	-0.165*	-0.294*	0.165*	-0.129*	0.294*	0.129*
	p	0.000	0.000	0.000	0.000	0.000	0.000
705	Ave	-0.113*	-0.228*	0.113*	-0.115*	0.228*	0.115*
	p	0.000	0.000	0.000	0.000	0.000	0.000
715	Ave	0.012	-0.071*	-0.012	-0.083*	0.071*	0.083*
	p	0.652	0.000	0.652	0.000	0.000	0.000
726	Ave	0.186*	0.176*	-0.186*	-0.011	-0.176*	0.011
	p	0.000	0.000	0.000	0.690	0.000	0.690
752	Ave	0.380*	0.350*	-0.380*	-0.030	-0.350*	0.030
	p	0.000	0.000	0.000	0.224	0.000	0.224
768	Ave	0.398*	0.391*	-0.398*	-0.007	-0.391*	0.007
	p	0.000	0.000	0.000	0.782	0.000	0.782
774	Ave	0.396*	0.402*	-0.396*	0.006	-0.402*	-0.006
	p	0.000	0.000	0.000	0.835	0.000	0.835
789	Ave	0.407*	0.419*	-0.407*	0.012	-0.419*	-0.012
	p	0.000	0.000	0.000	0.663	0.000	0.663
827	Ave	0.413*	0.398*	-0.103*	-0.016	-0.398*	0.016
	p	0.000	0.000	0.000	0.591	0.000	0.591
864	Ave	0.431*	0.367*	-0.431*	-0.064*	-0.367*	0.064*
	p	0.000	0.000	0.000	0.026	0.000	0.026
897	Ave	0.428*	0.355*	-0.428*	-0.073*	-0.355*	0.073*
	p	0.000	0.000	0.000	0.012	0.000	0.012
962	Ave	0.363*	0.269*	-0.363*	-0.094*	-0.269*	0.094*
	p	0.000	0.000	0.000	0.008	0.000	0.008
984	Ave	0.409*	0.276*	-0.409*	-0.133*	-0.276*	0.133*
	p	0.000	0.000	0.000	0.000	0.000	0.000

Note: The symbol * means the significance high than 0.05. (Ave – mean value; p – significant probability level)

Discussion

Impact of Background Factors on Diagnosis of Wheat Powdery Mildew

Several images of different disease severities are presented from Fig. 4a to Fig. 4d and Fig. 4e to Fig. 4h and growing stages are also shown from Fig. 4 (a, b, c and d) to Fig. 4 (e, f, g and h). As seen in Fig. 4, the disease diagnosis is related to wheat ear, healthy, diseased, and shadowed leaves, stem and soil. Therefore, the background factors could reduce the accuracy of disease assessment. It was pointed out that the inversion accuracy of plant nutrition estimation based on remote sensing could be improved after the reduction of background influences (Huete, 1988; Zhao *et al*., 2008; Chen *et al*., 2010). However, there are few studies on this issue for crop disease recognition and detection. This study investigated the influence of multiple background factors on diagnosis of wheat powdery mildew. The results showed that healthy and infected leaves have a high degree of recognition accuracy of 98.4%. The shadowed leaves were identified 100%, which indicated that they have very little impact on disease identification. However, wheat ears were often falsely being recognized as the infected leaves with the probability up to 15.9%. Thus, wheat ear is an important factor to reduce disease diagnosis accuracy and should be more concerned in disease monitoring by optical remote sensing.

Table 5: Recognition features between infected leaves and background factors

RVI				NDVI		REP
726 nm/689 nm	705 nm/694 nm	700 nm/679 nm	715 nm/705 nm	NIR	Red	Red edge area
679 nm/503 nm	715 nm/700 nm	962 nm/679 nm	827 nm/726 nm	768 nm	715 nm	
774 nm/679 nm	544 nm/503 nm	544 nm/423 nm	897 nm/503 nm	768 nm	705 nm	
768 nm/694 nm	726 nm/705 nm	864 nm/715 nm	984 nm/715 nm	774 nm	689 nm	
715 nm/694 nm	897 nm/544 nm	774 nm/503 nm	897 nm/752 nm	864 nm	700 nm	
962 nm/726 nm	694 nm/544 nm	726 nm/700 nm	694 nm/679 nm	897 nm	726 nm	
700 nm/508 nm	534 nm/508 nm	726 nm/715 nm	897 nm/534 nm	-	-	
679 nm/534 nm	705 nm/689 nm	752 nm/715 nm	774 nm/689 nm	-	-	
726 nm/544 nm	RVSI			-	-	

Table 6: Identification features of different disease severities

RVI				NDVI		REP
705 nm/694 nm	705 nm/689 nm	726 nm/679 nm	700 nm/534 nm	897 nm	726 nm	Red edge area;
705 nm/544 nm	897 nm/752 nm	715 nm/658 nm	984 nm/417 nm	768 nm	700 nm	
774 nm/417 nm	700 nm/679 nm	715 nm/705 nm	984 nm/726 nm	768 nm	715 nm	Red edge
679 nm/508 nm	689 nm/503 nm	700 nm/503 nm	726 nm/705 nm	768 nm	689 nm	position
768 nm/726 nm	700 nm/689 nm	705 nm/679 nm	768 nm/679 nm	864 nm	705 nm	
864 nm/544 nm	962 nm/715 nm	752 nm/715 nm	715 nm/534 nm	864 nm	726 nm	
897 nm/726 nm	864 nm/689 nm	827 nm/726 nm	789 nm/508 nm	-	-	
827 nm/544 nm	694 nm/679 nm	705 nm/508 nm	752 nm/726 nm	-	-	

Table 7: Recognition accuracy between infected leaves and background factors

Observed Value	Predicted Value				
	Diseased Samples	Healthy Samples	Shadowed Samples	Wheat Ear	Mapping Accuracy
Diseased Samples	1594	6	0	20	98.4%
Healthy Samples	8	492	0	0	98.4%
Shadowed Samples	0	0	583	0	100%
Wheat Ear	91	19	0	464	80.8%
User's Accuracy	94.2%	95.2%	100%	95.9%	-
Overall Accuracy	95.6%				
Kappa Coefficient	95.2%				

Table 8: Diagnosis accuracy of different disease severities

Observed value	Predicted value			
	Healthy samples	Mild infection	Moderate infection	Mapping accuracy
Healthy Samples	496	0	4	99.2%
Mild Infection	3	306	39	87.9%
Moderate Infection	1	142	1129	88.8%
User's Accuracy	99.2%	68.3%	96.3%	-
Overall Accuracy	91.1%			
Kappa Coefficient	84.6%			

At present, the field-scale crop disease diagnosis using the images acquired from space-borne and airborne are limited by the 1–30 m spatial resolution (Franke *et al*., 2008; Mewes *et al*., 2011; Mirik *et al*., 2011). Such remote sensing mainly focuses on large-scale monitoring and forecasting of crop diseases and it does not consider the impact of wheat ears on disease assessment. Non-imaging hyperspectral techniques have the advantages of hundreds of bands, which can sensitively detect crop stress (Muhammed, 2005; Feng *et al*., 2013). However, they still cannot reduce the impacts of soil and wheat ears on disease diagnosis with different background factors. Although some leaf-scale models of crop diseases have been built in the laboratory, the models still need to be verified in the field conditions (Yuan *et al*., 2013; Ashourloo *et al*., 2014; Huang *et al*., 2014).

To sum up, there has been a great progress in crop diseases diagnosis in the scale of leaf, canopy and field. However, still little attention has been paid for crop disease remote sensing under multiple background factors with the limitations of the observation instruments. Although this study qualitatively analyzed spectral differences of different background factors with the unification of image and spectra, the diagnosis model of wheat powdery mildew without the influence of wheat ear has not established due to limited sampling points. That is the problem we will focus on in the future.

Impact of Disease Severities Determination on Spray Control

Timely and accurately recognition of disease severities based

on remote sensing can provide decision support for site-specific crop disease treatment, which is especially important in reducing spray volume and improving pest control effect to serve for grain security. However, presently there is almost no guidance for spraying pesticides after recognizing crop disease severities from remote sensing observation. This situation might be caused by (1) low spatial resolution and large observation scale. Space-borne and airborne remote sensing is mainly used for large-scale monitoring and forecasting of crop diseases. It is easily to assess the loss caused by disease infestation in the severely infected period but not easily to provide right spray guidance in the optimal plant protection stage (Qin and Zhang, 2005; Mewes *et al*., 2011); (2) In order to obtain stable spectral responses of crop diseases, studies tended to conduct in the leaf scale in laboratory condition to get rid of the complex crop growth environment in the field. There have been quite a number of studies on early diagnosis of wheat powdery mildew but they were barely verified under the field conditions (Devadas *et al*., 2009; Huang *et al*., 2013; Ashourloo *et al*., 2014). This resulted in that the most of the previous studies cannot be used in spray control guidance.

In this study, disease severities (healthy, mild, and moderate) of wheat powdery mildew were diagnosed in the field using high-resolution and hyperspectral imaging. It showed that the recognition accuracy of moderate infection is 88.8% and the accuracy of mild infection is 87.9%, which illustrates that the different severities of wheat powdery mildew can be better identified. However, because mild infected samples are easy to falsely recognize as healthy and moderate infected samples, it is still a challenge to detect mild infection in the field. Similar results were also shown in other reported studies (Qin and Zhang, 2005; Huang *et al*., 2013). Therefore, in order to effectively direct spray control of wheat powdery mildew, data in the early-infected stage should be measured and collected.

Conclusion

In this study, a hyperspectral imager was used to detect wheat powdery mildew with considering the impacts of wheat ears and the leaves under shadow to identify infected and healthy plant leaves. Through comparing and extracting the identification features between wheat ears and shadowed, healthy and infected plant leaves, we found that shadowed leaves can be perfectly recognized while the healthy and infected leaves, wheat ears could be identified with the rates of 98.4, 98.4 and 80.8%, respectively. For identification of different disease severities, the healthy leaves have the highest accuracy of 99.2%, while moderately and mildly infected leaves were determined as 88.2 and 87.8%, respectively. Finally it was also found that wheat ears could affect identification accuracy of wheat powdery mildew. In overall, these results provide important helpful for the assessment of crop diseases in the field using optical remote sensing.

Acknowledgements

This project was financially supported by the National Natural Science Foundation of China (Grant No. 41301471, 41301505), China Postdoctoral Special Foundation (Grant No. 2013T60189) and International Postdoctoral Exchange Fellowship Program (Grant No. 20130043).

References

Ashourloo, D., M.R. Mobasheri and A. Huete, 2014a. Developing two spectral disease indices coretection of wheat leaf rust (Pucciniatriticina), *Remote Sens.*, 6: 4723–4740

Ashourloo, D., M.R. Mobasheri and A. Huete, 2014b. Evaluating the Effect of Different Wheat Rust Disease Symptoms on Vegetation Indices Using Hyperspectral Measurements. *Remote Sens.*, 6: 5107–5123

Ashourloo, D., M.R. Mobasheri and A. Huete, 2014c. Evaluating the effect of different wheat rust disease symptoms on vegetation indices using hyperspectral measurements. *Remote Sens.*, 6: 5107–5123

Chen, P.F., D. Haboudane, N. Tremblay, J.H. Wang, P. Vigneault and B.G. Li, 2010. New spectral indicator assessing the efficiency of crop nitrogen treatment in corn and wheat. *Remote Sens Environ.*, 114: 1987–1997

Devadas, R., D.W. Lamb, S. Simpfendorfer and D Backhouse, 2009. Evaluating ten spectral vegetation indices for identifying rust infection in individual wheat leaves. *Precis Agric.*, 10: 459–470

Feng, W., X.Y. Wang, X. Song, L. He, Y.H. Wang and T.C. Guo, 2013. Estimation of severity level of wheat powdery mildew based on canopy spectral reflectance. *Acta Agron. Sin.*, 39: 1469–1477

Field, A., 2013. *Discovering Statistics using SPSS*, 4th edition, p: 101. SAGE Publications Ltd., Los Angeles, California, USA

Franke, J., T. Mewes and G. Menz, 2008. Airborne hyperspectral imaging for the detection of powdery mildew in wheat. *Proceeding SPIE 7086, Imaging Spectrometry XIII*. 708609

Giese, H., S. Hippe-Sanwald, S. Somerville and J. Weller, 1997. Erysiphe graminis. *The Mycota V, Part B*, *Plant Relationships*, pp: 55–77. Carroll, G.C. and P. Tudzynski, (eds.). Springer-Verlag, Berlin, Germany

Haboudane, D., N. Tremblay, J.R. Miller and P. Vigneault, 2008. Remote estimation of crop chlorophyll content using spectral indices derived from hyperspectral data, *IEEE T Geosci. Remote.*, 46: 423–437

Huang, W., D.W. Lamb and Z. Niu, 2007. Identification of yellow rust in wheat using in-situ spectral reflectance measurements and airborne hyperspectral imaging. *Precis Agric.*, 8: 187–197

Huang, L.S., D.Y. Zhang, D. Liang, L. Yuan, J.L. Zhao, G.S. Hu, S.Z. Du and X.G. Xu, 2013. Continuous wavelet analysis for diagnosing stress characteristics of leaf powdery mildew. *Int. J. Agric. Biol.*, 15: 34–40

Huang, W.J., Q.S. Guan, J.H. Luo, J.C. Zhang, J.L. Zhao, D. Liang, L.S Huang and D.Y. Zhang, 2014. New optimized spectral indices for identifying and monitoring winter wheat diseases. *IEEE J-STARS*, 7: 2516–2524

Huang, L.S., S.C. Ju, J.L. Zhao, D.Y. Zhang, Q. Hong, L. Teng, F. Yang and Y. Zuo, 2015. Hyperspectral measurements for estimating vertical infection of yellow rust on winter wheat plant. *Int. J. Agric. Biol.*, 17: 1237–1242

Huete, A.R., 1988. A soil-adjusted vegetation index (SAVI), *Remote Sens Environ.*, 25: 295–309

Hemmateenejad, B., R. Miri and M. Elyasi, 2012. A segmented principal component analysis--regression approach to QSAR study of peptides. *J. Theor. Biol.*, 305: 37–44

Mahlein, A.K., E.C. Oerke, U. Steiner and H.W. Dehne, 2012. Recent advances in sensing plant diseases for precision crop protection. *Eur. J. Plant Pathol.*, 133: 197–209

Mewes, T., J. Franke and G. Menz, 2011. Spectral requirements on airborne hyperspectral remote sensing data for wheat disease detection. *Precis Agric.*, 12: 795–812

Mirik, M., D.C. Jones, J.A. Price, F. Workneh, R.J. Ansley, and C.M. Rush, 2011. Satellite remote sensing of wheat infected by wheat streak mosaic virus. *Plant Dis.*, 95: 4–12

Muhammed, H.H., 2005. Hyperspectral cop reflectance data for characterising and estimating fungal disease severity in wheat. *Biosyst. Eng.*, 91: 9–20

Mutka, A.M. and R.S. Bart, 2014. Image-based phenotyping of plant disease symptoms. *Front Plant Sci.*, 5: 734

Naidu, R.A., E.M. Perry and F.J. Pierce, 2009. The potential of spectral reflectance technique for the detection of grapevine leaf roll-associated virus-3 in two red-berried wine grape cultivars, *Comput. Electr. Agric.*, 66: 38–45

Ortiz, B.V., S.J. Thomson, Y. Huang, K.N. Reddy and W. Ding, 2011. Determination of differences in crop injury from aerial application of glyphosate using vegetation indices. *Comput. Electr. Agric.*, 77: 204–213

Qin, Z.H. and M.H. Zhang, 2005. Detection of rice sheath blight for in-season disease management using multispectral remote sensing. *Int. J. Appl. Earth Obs.*, 7: 115–128

Rokach, L. and O. Maimon, 2008. *Data Mining with Decision Trees: Theory and Applications*, p: 26. World Scientific Pub Co Inc

Yang, C.M., 2010. Assessment of the severity of bacterial leaf blight in rice using canopy hyperspectral reflectance, *Prec. Agric.*, 11: 61–81

Yuan, L., J.C. Zhang, J.L. Zhao, W.J. Huang and J.H. Wang, 2013. Differentiation of yellow rust and powdery mildew in winter wheat and retrieving of disease severity based on leaf level. *Spectrosc Spect Anal.*, 33: 1608–1614

Zhang, H., Y. Lan, C.P. Suh, J.K. Westbrook, W.C. Hoffmann, C. Yang and Y. Huang, 2013. Fusion of remotely sensed data from airborne and ground-based sensors to enhance detection of cotton plants. *Comput. Electr. Agric.*, 93: 55–59

Zhang, J.C., L. Yuan, J.H. Wang, J.H. Luo, S.Z. Du and W.J. Huang, 2012. Research progress of crop diseases and pests monitoring based on remote sensing. *Trans. Chin. Soc. Agric. Eng.,* 28: 1–11

Zhao, C.J., W.J. Huang and J.H. Wang, 2008. *Basis and Application of Quantitative Remote Sensing in Agriculture*. Science Press, Beijing, China

Zhao, J.L., L.S. Huang, W.J. Huang, D.Y. Zhang, L. Yuan, J.C. Zhang and D. Liang, 2014. Hyperspectral measurements of severity of stripe rust on individual wheat leaves. *Eur. J. Plant Pathol.*, 139: 407–417

(Received 21 January 2016; Accepted 03 March 2016)